Title

Effects of Familial Alzheimers Disease Mutations on the Assembly of a β-Hairpin Peptide Derived from Aβ16-36.

Journal

Biochemistry, 61(6)

Authors

McKnelly, Kate
Kreutzer, Adam
Howitz, William
et al.

Publication Date

2022-03-15

DOI

10.1021/acs.biochem.1c00664

Peer reviewed

Published in final edited form as:

Biochemistry. 2022 March 15; 61(6): 446–454. doi:10.1021/acs.biochem.1c00664.

Effects of Familial Alzheimer's Disease Mutations on the Assembly of a β-Hairpin Peptide Derived from $A\beta_{16-36}$

Kate J. McKnelly[1], **Adam G. Kreutzer**[1], **William J. Howitz**[1], **Katelyn Haduong**[1], **Stan Yoo**[1], **Candace Hart**[1], **James S. Nowick**[1,2,*]

[1]Department of Chemistry, University of California Irvine, Irvine, CA 92697, United States

[2]Department of Pharmaceutical Sciences, University of California Irvine, Irvine, CA 92697, United States

Abstract

Familial Alzheimer's disease (FAD) is associated with mutations in the β-amyloid peptide (Aβ) or the amyloid precursor protein (APP). FAD mutations of Aβ were incorporated into a macrocyclic peptide that mimics a β-hairpin to study FAD point mutations K16N, A21G, E22Δ, E22G, E22Q, E22K, and L34V and their effect on assembly, membrane destabilization, and cytotoxicity. The X-ray crystallographic structures of the four E22 mutant peptides reveal that the peptides assemble to form the same compact hexamer. SDS-PAGE experiments reveal that the mutant FAD peptides assemble as trimers or hexamers, with peptides that have greater positive charge assembling as more stable hexamers. Mutations that increase the positive charge also increase the cytotoxicity of the peptides and their propensity to destabilize lipid membranes.

Graphical Abstract

*Corresponding Author: jsnowick@uci.edu.

The Supporting Information is available free of charge on the ACS Publications website at http://pubs.acs.org/.
Procedures for peptide synthesis, cytotoxicity, dye leakage, SDS-PAGE, CD spectroscopy, size exclusion chromatography, and peptide crystallization; (2) details ofX-ray crystallographic data collection, processing, and refinement; (3) peptide characterization data. (PDF)

Crystallographic coordinates of peptides $\mathbf{1_{E22D}}$, $\mathbf{1_{E22G}}$, $\mathbf{1_{E22Q}}$, and $\mathbf{1_{E22K}}$ were deposited into the Protein Data Bank (PDB) with codes 7JQS, 7JQR, 7JQU, and 7JQT.

The authors declare no competing financial interests.

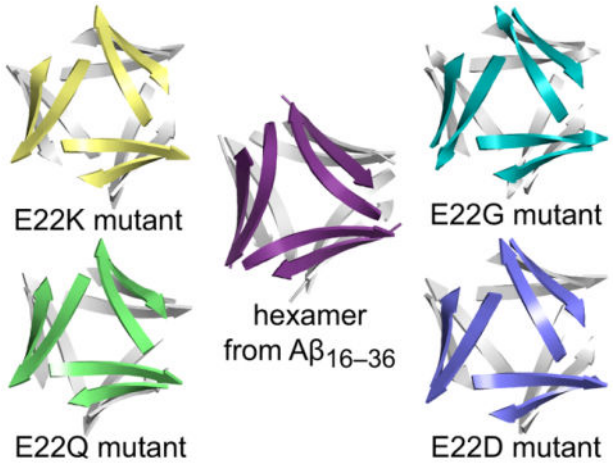

Introduction

Familial Alzheimer's disease (FAD) is insidious, because it results in the onset of the devastating neurodegeneration of Alzheimer's disease (AD) in individuals as young as age 30 and subsequent death at a young age.[1] Approximately 10–15% of early-onset FAD cases are caused by point mutations in the β-amyloid (Aβ) region of the amyloid precursor protein (APP).[2,3] These point mutations impact the oligomerization and fibrilization properties of Aβ, which can increase the cytotoxicity of these assemblies and exacerbate disease pathology. TEM images reveal that the Aβ mutations K16N, A21G, E22Δ, E22Q, E22K, and D23N induce the formation of amorphous aggregates, suggesting that these mutations cause an increase in Aβ oligomer formation.[5] The A21G and E22K Aβ mutants typically form very few fibrils, which are generally in short fibril bundles.[6] The E22Δ, E22Q, and L34V Aβ mutants have a higher propensity to form fibrils than wild type (WT) Aβ.[5] The E22G, E22Q, and E22K Aβ mutants exhibit greater cytotoxicity than WT Aβ, and the E22G and E22K Aβ mutants are thought to favor the formation of stable oligomers.[7,8] While these studies indicate that the FAD mutations of Aβ enhance aggregation and cytotoxicity, the relationship between the FAD mutations, oligomeric assembly, and cytotoxicity is poorly understood.

To better understand the structures and assembly of Aβ oligomers, our laboratory has pioneered macrocyclic peptides that constrain the central and *C*-terminal regions of Aβ in a β-hairpin conformation.[9–15] We previously studied macrocyclic β-hairpin peptide **1** which is composed of $Aβ_{16–22}$ and $Aβ_{30–36}$ β-strands linked together with two δ-linked ornithine (^{δ}Orn) turn units (Figure 1). Peptide **1** also contains an *N*-methyl group on the backbone of Phe19 to limit uncontrolled aggregation. Peptide **1** is thus designed to mimic an $Aβ_{16–36}$ β-hairpin.[13,16]

Peptide **1** assembles to form hexamers and is cytotoxic. The X-ray crystallographic structure of peptide **1** revealed that the peptide assembles to form a tightly packed hexamer.[13] A hexamer is also observed in SDS-PAGE. Cytotoxicity studies indicate that peptide **1** is toxic toward the human neuronal cell line SH-SY5Y.[13] Cytotoxicity of peptide **1** and its

propensity to form oligomers make it a suitable model system to study the effects of FAD point mutations in Aβ.

In the current study, we set out to gain insights into the effect of FAD mutations on the cytotoxicity, biophysical behavior, and assembly of Aβ, by preparing and studying derivatives of peptide **1** that contain known FAD mutations. Peptide **1** accommodates four FAD mutations at position 22 (E22Δ, E22G, E22Q, and E22K), as well as three other FAD mutations (K16N, A21G, and L34V). We prepared peptides $\mathbf{1_{E22D}}$, $\mathbf{1_{E22G}}$, $\mathbf{1_{E22K}}$, and $\mathbf{1_{E22Q}}$ to study the effect of a series of homologous mutations at position 22 (Figure 2). (The E22Δ mutation results in D23 in place of E22 and is thus designated E22D for the mutant peptide.) We also prepared and studied peptides $\mathbf{1_{K16N}}$, $\mathbf{1_{A21G}}$, and $\mathbf{1_{L34V}}$. Many of the FAD mutations to peptide **1** change the net charge of the peptide at neutral pH (Figure 2). Here we describe biological, biophysical, and structural studies of this series of peptide **1** mutants and discuss how the findings from these studies may help unravel the relationship between the FAD mutations, oligomeric assembly, and cytotoxicity.

Results

X-ray Crystallographic Studies of Peptides 1_{E22D}, 1_{E22G}, 1_{E22K}, and 1_{E22Q}.

X-ray crystallography reveals that peptides $\mathbf{1_{E22D}}$, $\mathbf{1_{E22G}}$, $\mathbf{1_{E22K}}$, and $\mathbf{1_{E22Q}}$ fold to form β-hairpins that assemble to form hexamers that are nearly identical to the hexamer formed by peptide **1** (Figure 3).[13] Upon screening the seven different mutants of peptide **1** in over 200 crystallization conditions, we found that only the E22 mutant peptides produced crystals suitable for X-ray diffraction, and we successfully solved the X-ray crystallographic structures of all E22 mutant peptides: $\mathbf{1_{E22D}}$, $\mathbf{1_{E22G}}$, $\mathbf{1_{E22K}}$, and $\mathbf{1_{E22Q}}$. Crystallization conditions and statistics for all crystal structures are in the Supplemental Information. We solved the X-ray crystallographic structure of peptide $\mathbf{1_{E22Q}}$ using molecular replacement with a crystallographically observed trimer of peptide **1** as a search model. We used SAD phasing to solve the X-ray crystallographic structure of peptide $\mathbf{1_{E22G}}$, and then used the monomer from the asymmetric unit of the peptide $\mathbf{1_{E22G}}$ crystal structure as a search model in molecular replacement to solve the structures of peptides $\mathbf{1_{E22D}}$ and $\mathbf{1_{E22K}}$. The hexamers formed by peptide **1** and the E22 mutant peptides consist of a dimer of triangular trimers with a hydrophobic core composed of six copies of the side chains of Leu_{17}, Phe_{19}, Ala_{21}, Ile_{31}, and Met_{35}.[13] All residues at position 22 are solvent exposed and do not contribute significantly to the assembly of the hexamers. The close similarity between the hexamers formed by these mutants and peptide **1** indicates that peptide **1** can accommodate known FAD mutations at position E22 without substantially altering oligomer formation.

Cytotoxicity.

To assess the cytotoxicity of the E22 mutant peptides, we treated human neuroblastoma SH-SY5Y cells with varying concentrations of the peptides and measured LDH release, a marker for cytotoxicity (Figure 4).[13,17] Peptides **1** and $\mathbf{1_{E22D}}$ proved the least toxic, exhibiting toxicity at 50 μM. Peptides $\mathbf{1_{E22G}}$ and $\mathbf{1_{E22Q}}$ are more toxic, exhibiting toxicity at 25 μM. Peptide $\mathbf{1_{E22K}}$ is the most toxic, exhibiting toxicity at 12.5 μM. Thus, the cytotoxicity increases ca. two-fold with each additional positive charge: **1** (+2) ≈ $\mathbf{1_{E22D}}$

(+2) < **1**$_{\mathbf{E22G}}$ (+3) ≈ **1**$_{\mathbf{E22Q}}$ (+3) < **1**$_{\mathbf{E22K}}$ (+4). This correlation between peptide charge and cytotoxicity suggests that the charge of mutant Aβ may play a pivotal role in cytotoxicity, with mutations that introduce greater positive charge causing greater cytotoxicity.

Membrane Disruption.

The correlation between positive charge and cytotoxicity of the E22 mutant peptides suggests a mechanism of toxicity in which the cationic peptides interact with and disrupt the cell membranes, a trend that has been observed with peptides containing multiple positively charged residues.[18–20] To investigate the disruption of membranes by the E22 mutant peptides, we performed dye leakage assays.[21,22] In these assays, large unilamellar vesicles (LUVs) — prepared in buffer to encapsulate a fluorescent dye — are exposed to varying concentrations of mutant peptide. If mutant peptides destabilize the membranes, the encapsulated dye leaks from the LUVs and is detected spectrofluorometrically as an increase in fluorescence.

All of the E22 mutant peptides cause dye leakage from negatively charged 1:1 phosphatidylcholine:phosphatidylserine (PC:PS) LUVs (Figure 5). Peptides **1** and **1**$_{\mathbf{E22D}}$ have EC_{50} values of 4.41 μM and 3.50 μM respectively. Peptides **1**$_{\mathbf{E22G}}$ and **1**$_{\mathbf{E22Q}}$ have EC_{50} values of 1.85 μM and 0.93 μM, which are about half those of peptides **1** and **1**$_{\mathbf{E22D}}$. Peptide **1**$_{\mathbf{E22K}}$ is the most active, with an EC_{50} value of 0.19 μM, which is approximately one order of magnitude smaller than those of peptides **1**, **1**$_{\mathbf{E22D}}$, **1**$_{\mathbf{E22G}}$ and **1**$_{\mathbf{E22Q}}$ (Figure 5). The trend in dye-leakage activity of the mutant peptides correlates with their cytotoxicity by LDH release assays: Peptides **1** and **1**$_{\mathbf{E22D}}$ (each with a charge of +2) are least destabilizing of the LUVs and least cytotoxic; peptides **1**$_{\mathbf{E22G}}$ and **1**$_{\mathbf{E22Q}}$ (each with a charge of +3) are more destabilizing and more cytotoxic; peptide **1**$_{\mathbf{E22K}}$ (with a charge of +4) is most destabilizing and most cytotoxic. Thus, the mutant peptides bearing greater positive charge exhibit greater interaction with and destabilization of the anionic PC:PS LUVs.

To further probe the role of charge in the interactions between the mutant peptides and the LUVs, we performed dye leakage assays with the E22 mutant peptides and LUVs composed of neutrally charged PC lipids. Peptides **1**, **1**$_{\mathbf{E22D}}$, **1**$_{\mathbf{E22G}}$, **1**$_{\mathbf{E22Q}}$, and **1**$_{\mathbf{E22K}}$ cause less dye leakage from neutrally charged PC LUVs than from negatively charged PC:PS LUVs by ca. one order of magnitude, with EC_{50} values greater than 10 μM (Figure 5). The weaker interactions with the neutral LUVs further support a model in which charge plays a large role in the interactions of the peptides with cellular membranes.

Oligomerization in SDS.

To probe the assembly of the E22 mutant peptides in an anionic lipid environment, we turned to SDS-PAGE. Peptide **1** was previously reported to migrate as a hexamer in SDS-PAGE.[13] We ran the E22 mutants and peptide **1** on SDS-PAGE and visualized the bands with silver staining to compare the assembly of the peptides. Peptides **1**, **1**$_{\mathbf{E22D}}$, **1**$_{\mathbf{E22G}}$, **1**$_{\mathbf{E22K}}$, and **1**$_{\mathbf{E22Q}}$, which all have molecular weights of ca. 1.8 kDa, all migrate as bands at roughly 10 kDa (Figure 6). Although there are some small differences among the positions of the bands formed by peptide **1** and the E22 mutants, all are roughly consistent with the molecular weight expected for hexamers (ca. 10.6 kDa), although oligomers of other

sizes (e.g. 4–8-mers) cannot be ruled out. The bands differ in appearance, with peptides **1** and $\mathbf{1_{E22D}}$ forming comet-shaped bands that streak downward, and peptides $\mathbf{1_{E22G}}$, $\mathbf{1_{E22Q}}$, and $\mathbf{1_{E22K}}$ forming more compact bands. The streaky appearance of the bands formed by peptides **1** and $\mathbf{1_{E22D}}$ may reflect that the hexamers formed by these peptides are less stable, equilibrating with monomer or lower-order oligomers as these less charged (+2) peptides migrate through the gel. The hexamers formed by peptides $\mathbf{1_{E22G}}$, $\mathbf{1_{E22K}}$, and $\mathbf{1_{E22Q}}$ are more stable, with less propensity to equilibrate with monomer or lower order oligomers. These observations suggest that the anionic SDS better stabilizes the more positively charged hexamers formed by the more positively charged mutants.

To further assess the relative stabilities of the hexamers formed by peptides **1**, $\mathbf{1_{E22D}}$, $\mathbf{1_{E22G}}$, $\mathbf{1_{E22K}}$, and $\mathbf{1_{E22Q}}$ in SDS-PAGE, we ran peptide **1** and each of the E22 mutants at varying concentrations (Figure 7). Peptide $\mathbf{1_{E22K}}$ appears as a compact band at concentrations ranging from 0.2 mg/mL to 0.025 mg/mL, with no variation in position of the lower edge of each band and little shift in the upper edge of the band as the concentration decreases. The lower edge of each band aligns with the 10 kDa ladder band, consistent with the formation of a hexamer (10.6 kDa). Peptides **1**, $\mathbf{1_{E22D}}$, $\mathbf{1_{E22G}}$, and $\mathbf{1_{E22Q}}$ stained less intensely in these experiments and were thus run at concentrations ranging from 0.4 mg/mL to 0.05 mg/mL. Peptides **1** and $\mathbf{1_{E22D}}$ appear as less compact bands, with no variation in position of the lower edge of each band but substantial variation in the upper edge. The lower edge of each band falls between the 10 kDa and 4.6 kDa ladder bands, suggesting an equilibrium favoring a lower order oligomer at lower concentrations. Peptides $\mathbf{1_{E22G}}$ and $\mathbf{1_{E22Q}}$ also appear as less compact bands, with the lower edge of each band falling somewhat below the 10 kDa ladder band. Collectively, these concentration-based SDS-PAGE experiments suggest that the hexamers formed by peptide $\mathbf{1_{E22K}}$ are most stable, with decreasing stability of the hexamers correlating with decreasing net charge: $\mathbf{1_{E22K}}$ (+4) > $\mathbf{1_{E22G}}$ (+3) ≈ $\mathbf{1_{E22Q}}$ (+3) > $\mathbf{1_{E22D}}$ (+2) ≈ **1** (+2).

Folding.

The crystallographic oligomers formed by peptides 1, $\mathbf{1_{E22D}}$, $\mathbf{1_{E22G}}$, $\mathbf{1_{E22Q}}$, and $\mathbf{1_{E22K}}$ are composed of folded β-hairpins. To determine if the mutant peptides fold in a similar fashion in aqueous solution, we performed circular dichroism (CD) spectroscopy.[24,25] The CD spectra reveal that peptides **1**, $\mathbf{1_{E22D}}$, $\mathbf{1_{E22G}}$, $\mathbf{1_{E22Q}}$, and $\mathbf{1_{E22K}}$ all exhibit some β-sheet character (Figure 8). Peptides **1** and $\mathbf{1_{E22D}}$ primarily show canonical β-sheet character by CD, as indicated by minima at ~218 nm. Peptides **1** and $\mathbf{1_{E22D}}$ have additional dips at ~190 nm, indicating that the peptides also have partial random coil character. Peptides $\mathbf{1_{E22G}}$ and $\mathbf{1_{E22Q}}$ have two dips, with minima at ~218 nm and ~190–200 nm, indicating that the peptides have significant random coil character in addition to β-sheet character. Peptide $\mathbf{1_{E22K}}$ has a broad minimum from ~205–215 nm, also suggesting the presence of both β-sheet and random coil character. Collectively, the CD spectra suggest that peptides with similar charge have similar folding patterns, with the peptides with +2 charge (**1** and $\mathbf{1_{E22D}}$) exhibiting the greatest degree of β-sheet folding in solution.

Assembly in Solution.

To investigate how the E22 mutant peptides assemble in aqueous solution, we turned to size exclusion chromatography (SEC). We ran cytochrome c (12.4 kDa), aprotinin (6.5 kDa), and vitamin B_{12} (1.3 kDa) as molecular weight markers in these experiments, to help determine whether the peptides (ca. 1.8 kDa each) ran as monomers or oligomers. Peptide $\mathbf{1_{E22K}}$ (+4) elutes as a single peak at 20.5 mL (Figure 9C). The peak elutes after the vitamin B_{12} size standard (19.5 mL) and tails beyond 25 mL, suggesting that the peptide runs as a monomer but sticks to the column. Peptide $\mathbf{1_{E22G}}$ shows a major peak at 22.0 mL, but also show smaller peaks at 19.5 and 17.5 mL (Figure 9B). These peaks elute after the aprotinin size standard (16.0 mL), suggesting the presence of dimer and trimer, in addition to monomer. Peptide $\mathbf{1_{E22Q}}$ also shows a major peak at 22.3 mL and somewhat smaller peaks at 19.5 and 17.5 mL, suggesting the presence of monomer, dimer, and trimer (Figure 9B). Peptide **1** (+2) also shows three peaks (19.3, 17.5, and 16.2 mL), suggesting the presence of monomer, dimer, and trimer (Figure 9A). Peptide $\mathbf{1_{E22D}}$ (+2) shows only two peaks (19.8 and 17.8 mL), suggesting the presence of monomer and dimer or trimer (Figure 9A).

In contrast to SDS-PAGE, none of the peptides appear to run as hexamers in SEC, and the most highly charged peptide, $\mathbf{1_{E22K}}$, exhibits the least self-assembly. In SDS-PAGE, the amphiphilic dodecylsulfate anion appears to facilitate the assembly of the more cationic peptides, while in aqueous solution, the most charged peptide is mostly or completely monomeric.

Peptides 1_{K16N}, 1_{A21G}, and 1_{L34V}.

We studied peptides $\mathbf{1_{K16N}}$, $\mathbf{1_{A21G}}$, and $\mathbf{1_{L34V}}$ in a similar fashion to peptide **1** and the E22 mutant peptides. None of these peptides afforded crystals suitable for X-ray crystallography. Cytotoxicity, membrane disruption, and SEC studies of peptides $\mathbf{1_{K16N}}$ and $\mathbf{1_{L34V}}$ were limited by poor solubility. For these reasons, studies of peptides $\mathbf{1_{K16N}}$, $\mathbf{1_{A21G}}$, and $\mathbf{1_{L34V}}$ were less illuminating than studies of the E22 mutants.

Peptide $\mathbf{1_{A21G}}$ (+2) proved toxic toward SH-SY5Y cells at 50 uM as assessed by an LDH-release assay (Figure 10A). Peptides $\mathbf{1_{k16N}}$ (+1) and $\mathbf{1_{L34V}}$ (+2) showed no toxicity at 50 uM when the peptides were prepared in water or in DMSO (Figures 10A and S1). Peptides $\mathbf{1_{K16N}}$ and $\mathbf{1_{L34V}}$ exhibited poor solubility in water and in buffer. We attempted to mitigate the peptide insolubilities by preparing peptides $\mathbf{1_{K16N}}$ and $\mathbf{1_{L34V}}$ in DMSO. When the DMSO stock solutions were diluted into the culture media, precipitation was not observed. Nevertheless, it was not possible to determine whether the peptides were fully solubilized in the assay media by this procedure and whether the cells received exposure to 50 uM of the peptide. Thus, the lack of apparent toxicity of peptide $\mathbf{1_{K16N}}$ might reflect either the low (+1) charge of this peptide or its poor solubility. The lack of apparent toxicity of peptide $\mathbf{1_{L34V}}$ is surprising because peptide $\mathbf{1_{L34V}}$ is identical in charge to peptides **1**, $\mathbf{1_{E22D}}$, and $\mathbf{1_{A21G}}$, and the leucine-to-valine mutation differs only by a single methylene group. The poor solubility of peptide $\mathbf{1_{L34V}}$ may account for its apparent lack of toxicity.

Peptide $\mathbf{1_{A21G}}$ proved more destabilizing of PC:PS LUVs than the other peptides bearing +2 charge (EC_{50} = 1.9 μM, vs. 4.4 μM for peptide **1** and 3.5 μM for peptide $\mathbf{1_{E22D}}$). The

EC_{50} of peptide $\mathbf{1_{A21G}}$ is comparable to the +3 charged peptide $\mathbf{1_{E22G}}$, albeit less than the +3 charged peptide $\mathbf{1_{E22Q}}$ (Figures 5 & 10B). Peptides $\mathbf{1_{K16N}}$ (+1) and $\mathbf{1_{L34V}}$ (+2) do not cause membrane destabilization as readily as the other mutant peptides (EC_{50} ~ 12 μM). The lower solubilities of these peptides or lower charge of peptide $\mathbf{1_{K16N}}$ (+1) may account for the modest activity of these peptides.

Peptides $\mathbf{1_{A21G}}$, $\mathbf{1_{K16N}}$, and $\mathbf{1_{L34V}}$ assemble to form oligomers in the presence of SDS (Figure 10C). When run at a concentration of 0.4 mg/mL, peptides $\mathbf{1_{A21G}}$ (+2) and $\mathbf{1_{L34V}}$ (+2) migrate as comet-shaped bands that approach the 10 kDa ladder band. At 0.4 mg/mL, peptide $\mathbf{1_{KI6N}}$ (+1) migrates between the 4.6 and 10 kDa ladder bands. As seen with other mutant peptides that have a net charge of +3 or lower, peptide $\mathbf{1_{A21G}}$ (+2) also migrates as bands that decrease in apparent MW upon decrease in peptide concentration, from 0.4 mg/mL to 0.2, 0.1, and 0.05 mg/mL.

Peptides $\mathbf{1_{A21G}}$, $\mathbf{1_{L34V}}$, and $\mathbf{1_{K16N}}$ have β-sheet character by CD spectroscopy, as all these mutant peptide spectra have bands with minima at ~218 nm (Figure 10D). Peptide $\mathbf{1_{L34V}}$ appears to have the greatest β-sheet character, as the spectra has only one band at ~218 nm. Peptides $\mathbf{1_{A21G}}$ and $\mathbf{1_{K16N}}$ both have additional dips at ~190 nm, indicating that the peptides also have random coil character.

Peptide $\mathbf{1_{A21G}}$ shows two peaks (19.2 mL and 17.7 mL) by SEC (Figure 10E), and peptides $\mathbf{1_{L34V}}$ and $\mathbf{1_{KI6N}}$ were not run on SEC because the peptides were insoluble in the column running buffer. The peaks of peptide $\mathbf{1_{A21G}}$ suggest the presence of monomer and dimer or trimer, similar to other mutant peptides with a charge of +2.

Discussion

Although familial mutations of Aβ result in dramatic differences in the onset of Alzheimer's disease, incorporation of several of these mutations into a β-hairpin peptide derived from $Aβ_{16–36}$ does not result in dramatic differences in behavior of the peptides. Peptides containing each of the four familial mutations at position 22 assemble to form similar hexamers in the crystal state and appear to assemble to form hexamers in the lipid environment provided by SDS-PAGE. Three of the four E22 mutant hexamers have greater net positive charge and appear to be more stable in lipid environments than those formed by the wild type peptide **1**. The more positively charged E22 mutants also interact more strongly with lipids and are more toxic toward cells. These differences may reflect differences in behavior of the hexamers, although interactions of the monomers cannot be excluded.

The differences observed among the E22 mutants may shed light on the differences in behavior of the corresponding familial mutants of full-length Aβ. Most notable among the differences in the E22 mutants is the disruption of lipid bilayer membranes of anionic LUVs. Mechanisms of cytotoxicity caused by oligomers of full-length Aβ are thought to involve disruption of membrane integrity, calcium dysregulation, and pore formation.[26–36] We envision that peptides **1**, $\mathbf{1_{E22D}}$, $\mathbf{1_{E22G}}$, $\mathbf{1_{E22K}}$, and $\mathbf{1_{E22Q}}$ may cause membrane destabilization and cytotoxicity through similar mechanisms — insertion into membranes

as hexamers or the corresponding dimer or trimer subunits, followed by disruption of membrane integrity.

The changes in charge among the E22 mutants mirror changes in charge of mutants of full-length Aβ. Although Aβ has a net negative charge at physiological pH (~7.4), many of the mutations in FAD make the net charge of Aβ less negative. These differences in charge are significant, because the charged state of a peptide dictates how it can associate with and destabilize cell membranes. Aβ is calculated to have a charge of ca. −3 at physiological pH.[37] Six out of the twelve FAD mutations of Aβ (D7N, E11K, E22G, E22K, E22Q, and D23N) involve the loss of an acidic residue in exchange for a neutral or basic residue. One FAD mutation (E22Δ) is simply a deletion of an acidic residue without replacement. All of these mutations thus cause a one- or two-unit diminution in the negative charge of Aβ, from −3 to −2 or −1.[37] Only two FAD mutations (H6R and K16N) occur at basic residues, which are replaced with another basic residue or a neutral residue, resulting in no change or a greater negative charge. The remaining three FAD mutations (A2V, A21G, and L34V) involve the exchange of a neutral residue for a neutral residue. Thus, over half of the FAD mutations make the net charge of the Aβ peptide less negative and can increase the propensity of the peptide to associate with cell membranes.

Oligomers of Aβ are thought to be central to the neurodegeneration in Alzheimer's disease.[38,39] The model system provided by the macrocyclic β-hairpin peptides in this study offers a window into the oligomerization of Aβ bearing a variety of familial mutations. It should, of course, be noted that the model system has a number of limitations, because it contains conformational constraints and lacks key residues that comprise Aβ. For example, it lacks Lys_{28}, which could form a salt bridge with GIU_{22} or Asp_{23} in full-length Aβ. Furthermore, the conformational constraints provided by macrocyclization limit the potential to form alternative hydrogen-bonding patterns, shift the registration of the paired amino acids, or switch of solvent-exposed residues. Nevertheless, the model system allows comparison of the effects of the familial mutations upon oligomerization with a level of detail and control that would not be possible with full-length Aβ.

Conclusions

Macrocyclic β-hairpin peptides derived from $Aβ_{16–36}$ allow the mimicry of many of the known familial mutants of Aβ and exhibit meaningful trends among the closely related E22 mutants. The E22 mutations change the net charge of the peptides but do not alter the propensity of the peptides to assemble as hexamers in the solid state or to form hexamers in the lipid environment of SDS. Instead, changing the net charge of the peptides alters the degree of interaction of the peptide with lipid membranes, leading to greater activity in dye-leakage assays and greater cytotoxicity. In aqueous solution, the E22 mutant peptides do not appear to form well defined oligomers and exhibit variable degrees of β-sheet folding. The K16N, A21G, and L34V mutant peptides offered less meaningful insights than the E22 mutants.

The hexamers formed by the E22 mutant peptides parallel the observation of hexamers of biogenic Aβ and the corresponding E22 mutants in SDS-PAGE.[40] Although the structures of

the hexamers formed by full-length Aβ peptides are not known, a variety of studies suggest that β-hairpins are building blocks of some Aβ oligomers.[41–43] The lipid environments provided by SDS and LUVs arguably provide more biologically relevant systems in which to study Aβ and peptides derived from Aβ than purely aqueous environments, because lipids constitute 50% of the dry weight of the brain and the amyloid precursor protein from which Aβ is generated is membrane-bound.[44–46] Our findings from studying the E22 mutant peptides may provide clues about why these mutants lead to enhanced neurodegeneration in FAD, as they suggest a greater degree of interaction of the mutant peptides or their oligomeric assemblies with the membranes of neurons and other cells in the brain.

Supplementary Material

Refer to Web version on PubMed Central for supplementary material.

Acknowledgements

The authors would like to thank Mohamed Laayouni, Anne-Marie Leiby, and Mia G. Russo, for help in preliminary studies. We thank the National Institutes of Health (NIH) National Institute of General Medical Sciences (NIGMS) for funding (Grant GM097562) and the National Institute on Aging (Grant RF1AG072587).

References

(1). 2020 Alzheimer's Disease Facts and Figures. Alzheimers. Dement 2020. 10.1002/alz.12068.

(2). Selkoe DJ Alzheimer's Disease: Genes, Proteins, and Therapy. Physiol. Rev 2001, 81 (2), 741–766. [PubMed: 11274343]

(3). Weggen S; Beher D Molecular Consequences of Amyloid Precursor Protein and Presenilin Mutations Causing Autosomal-Dominant Alzheimer's Disease. Alzheimers. Res. Ther 2012, 4 (2), 9. [PubMed: 22494386]

(4). Benilova I; Karran E; De Strooper B The Toxic Aβ Oligomer and Alzheimer's Disease: An Emperor in Need of Clothes. Nat. Neurosci 2012, 15 (3), 349–357. [PubMed: 22286176]

(5). Hatami A; Monjazeb S; Milton S; Glabe CG Familial Alzheimer's Disease Mutations within the Amyloid Precursor Protein Alter the Aggregation and Conformation of the Amyloid-β Peptide. J. Biol. Chem 2017, 292 (8), 3172–3185. [PubMed: 28049728]

(6). Hubin E; Deroo S; Schierle GK; Kaminski C; Serpell L; Subramaniam V; van Nuland N; Broersen K; Raussens V; Sarroukh R Two Distinct β-Sheet Structures in Italian-Mutant Amyloid-Beta Fibrils: A Potential Link to Different Clinical Phenotypes. Cell. Mol. Life Sci 2015, 72 (24), 4899–4913. [PubMed: 26190022]

(7). Nilsberth C; Westlind-Danielsson A; Eckman CB; Condron MM; Axelman K; Forsell C; Stenh C; Luthman J; Teplow DB; Younkin SG; Näslund J; Lannfelt L The "Arctic" APP Mutation (E693G) Causes Alzheimer's Disease by Enhanced Aβ Protofibril Formation. Nat. Neurosci 2001, 4, 887–893. [PubMed: 11528419]

(8). Masuda Y; Nakanishi A; Ohashi R; Takegoshi K; Shimizu T; Shirasawa T; Irie K Verification of the Intermolecular Parallel β-Sheet in E22K-Aβ42 Aggregates by Solid-State NMR Using Rotational Resonance: Implications for the Supramolecular Arrangement of the Toxic Conformer of Aβ42. Biosci. Biotechnol. Biochem 2008, 72 (8), 2170–2175. [PubMed: 18685204]

(9). Pham JD; Chim N; Goulding CW; Nowick JS Structures of Oligomers of a Peptide from β-Amyloid. J. Am. Chem. Soc 2013, 135 (33), 12460–12467. [PubMed: 23927812]

(10). Spencer RK; Li H; Nowick JS X-Ray Crystallographic Structures of Trimers and Higher-Order Oligomeric Assemblies of a Peptide Derived from $A\beta_{17–36}$. J. Am. Chem. Soc 2014, 136 (15), 5595–5598. [PubMed: 24669800]

(11). Kreutzer AG; Hamza IL; Spencer RK; Nowick JS X-Ray Crystallographic Structures of a Trimer, Dodecamer, and Annular Pore Formed by an $A\beta_{17–36}$ β-Hairpin. J. Am. Chem. Soc 2016, 128 (13), 4634–4642.

(12). Salveson PJ; Spencer RK; Kreutzer AG; Nowick JS X-Ray Crystallographic Structure of a Compact Dodecamer from a Peptide Derived from $A\beta_{16–36}$. Org. Lett 2017, 19 (13), 3462–3465. [PubMed: 28683555]

(13). Kreutzer AG; Spencer RK; McKnelly KJ; Yoo S; Hamza IL; Salveson PJ; Nowick JS A Hexamer of a Peptide Derived from $A\beta_{16–36}$. Biochemistry 2017, 56 (45), 6061–6071. [PubMed: 29028351]

(14). Kreutzer AG; Yoo S; Spencer RK; Nowick JS Stabilization, Assembly, and Toxicity of Trimers Derived from Aβ. J. Am. Chem. Soc 2017, 139 (2), 966–975. [PubMed: 28001392]

(15). Kreutzer AG; Nowick JS Elucidating the Structures of Amyloid Oligomers with Macrocyclic β-Hairpin Peptides: Insights into Alzheimer's Disease and Other Amyloid Diseases. Acc. Chem. Res 2018, 51 (3), 706–718. [PubMed: 29508987]

(16). Nowick JS; Lam KS; Khasanova TV; Kemnitzer WE; Maitra S; Mee HT; Liu R An Unnatural Amino Acid That Induces β-Sheet Folding and Interaction in Peptides. J. Am. Chem. Soc 2002, 124 (18), 4972–4973. [PubMed: 11982357]

(17). Korzeniewski C; Callewaert DM An Enzyme-Release Assay for Natural Cytotoxicity. J. Immunol. Methods 1983, 64 (3), 313–320. [PubMed: 6199426]

(18). Terzi E; Hölzemann G; Seelig J Alzheimer Beta-Amyloid Peptide 25–35: Electrostatic Interactions with Phospholipid Membranes. Biochemistry 1994, 33 (23), 7434–7441. [PubMed: 8003508]

(19). Jiang Z; Vasil AI; Hale JD; Hancock REW; Vasil ML; Hodges RS Effects of Net Charge and the Number of Positively Charged Residues on the Biological Activity of Amphipathic Alpha-Helical Cationic Antimicrobial Peptides. Biopolymers 2008, 90 (3), 369–383. [PubMed: 18098173]

(20). Huang Y; Huang J; Chen Y Alpha-Helical Cationic Antimicrobial Peptides: Relationships of Structure and Function. Protein Cell 2010, 1 (2), 143–152. [PubMed: 21203984]

(21). Arias M; Vogel HJ Fluorescence and Absorbance Spectroscopy Methods to Study Membrane Perturbations by Antimicrobial Host Defense Peptides. Methods Mol. Biol 2017, 1548, 141–157. [PubMed: 28013502]

(22). Salveson PJ; Haerianardakani S; Thuy-Boun A; Kreutzer AG; Nowick JS Controlling the Oligomerization State of Aβ-Derived Peptides with Light. J. Am. Chem. Soc 2018, 140 (17), 5842–5852. [PubMed: 29627987]

(23). Simpson RJ Staining Proteins in Gels with Silver Nitrate. CSH Protoc. 2007, 2007, db.prot4727.

(24). Kelly SM; Jess TJ; Price NC How to Study Proteins by Circular Dichroism. Biochim. Biophys. Acta 2005, 1751 (2), 119–139. [PubMed: 16027053]

(25). Greenfield NJ Using Circular Dichroism Spectra to Estimate Protein Secondary Structure. Nat. Protoc 2006, 1 (6), 2876–2890. [PubMed: 17406547]

(26). Arispe N; Pollard HB; Rojas E Zn2+ Interaction with Alzheimer Amyloid Beta Protein Calcium Channels. Proc. Natl. Acad. Sci. U.S. A 1996, 93 (4), 1710–1715. [PubMed: 8643694]

(27). Lin H; Zhu YJ; Lai R Amyloid β Protein (1–40) Forms Calcium-Permeable, Zn^{2+} - Sensitive Channel in Reconstituted Lipid Vesicles†,‡. Biochemistry. 1999, 38 (34), 11189–11196. [PubMed: 10460176]

(28). Ho R; Ortiz D; Shea TB Amyloid-Beta Promotes Calcium Influx and Neurodegeneration via Stimulation of L Voltage-Sensitive Calcium Channels rather than NMDA Channels in Cultured Neurons. J. Alzheimers. Dis 2001, 3 (5), 479–483. [PubMed: 12214034]

(29). Demuro A; Mina E; Kayed R; Milton SC; Parker I; Glabe CG Calcium Dysregulation and Membrane Disruption as a Ubiquitous Neurotoxic Mechanism of Soluble Amyloid Oligomers. J. Biol. Chem 2005, 280 (17), 17294–17300. [PubMed: 15722360]

(30). Small DH; Gasperini R; Vincent AJ; Hung AC; Foa L The Role of Aβ-Induced Calcium Dysregulation in the Pathogenesis of Alzheimer's Disease. J. Alzheimers. Dis 2009, 16 (2), 225–233. [PubMed: 19221414]

(31). Kagan BL; Thundimadathil J Amyloid Peptide Pores and the Beta Sheet Conformation. Adv. Exp. Med. Biol 2010, 677, 150–167. [PubMed: 20687488]

(32). Demuro A; Parker I; Stutzmann GE Calcium Signaling and Amyloid Toxicity in Alzheimer Disease. J. Biol. Chem 2010, 285 (17), 12463–12468. [PubMed: 20212036]

(33). Di Scala C; Yahi N; Boutemeur S; Flores A; Rodriguez L; Chahinian H; Fantini J Common Molecular Mechanism of Amyloid Pore Formation by Alzheimer's β-Amyloid Peptide and α-Synuclein. Sci. Rep 2016, 6, 28781. [PubMed: 27352802]

(34). Sciacca MFM; Kotler SA; Brender JR; Chen J; Lee D; Ramamoorthy A Two-step mechanism of membrane disruption by Aβ through membrane fragmentation and pore formation. Biophys J. 2012, 103 (4), 702–710. [PubMed: 22947931]

(35). Kotler SA; Walsh P; Brender JR; Ramamoorthy A Differences between amyloid-β aggregation in solution and on the membrane: insights into elucidation of the mechanistic details of Alzheimer's diseas. Chem. Soc. Rev 2014, 43, 6692–6700. [PubMed: 24464312]

(36). Fatafta H; Kav B; Bundschuh BF; Loschwitz J; Strodel B Disorder-to-order transition of the amyloid-β peptide upon lipid binding. Biophys. Chem 2022, 280, 106700. [PubMed: 34784548]

(37). Kozlowski LP IPC isoelectric point calculator http://isoelectric.org/calculate.php (accessed Nov 30, 2020).

(38). Nguyen PH; Ramamoorthy A; Sahoo BR; Zheng J; Faller P; Straub JE; Dominguez L; Shea J-E; Dokholyan NV; De Simone A; Ma B; Nussinov R; Najafi S; Ngo ST; Loquet A; Chiricotto M; Ganguly P; McCarty J; Li MS; Hall C; Wang Y; Miller Y; Melchionna S; Habenstein B; Timr S; Chen J; Hnath B; Strodel B; Kayed R; Lesné S; Wei G; Sterpone F; Doig AJ; and Derreumaux P Amyloid Oligomers: A Joint Experimental/Computational Perspective on Alzheimer's Disease, Parkinson's Disease, Type II Diabetes, and Amyotrophic Lateral Sclerosis. Chem. Rev 2021, 121 (4), 2545–2647. [PubMed: 33543942]

(39). Cawood EE; Karamanos TK; Wilson AJ; Radford SE Visualizing and trapping transient oligomers in amyloid assembly pathways. Biophys. Chem 2021, 268, 106505. [PubMed: 33220582]

(40). Vadukul DM; Vrancx C; Burguet P; Contino S; Suelves N; Serpell LC; Quinton L; Kienlen-Campard P An Evaluation of the Self-Assembly Enhancing Properties of Cell-Derived Hexameric Amyloid-β. Sci. Rep 2021, 11 (1), 11570. [PubMed: 34078941]

(41). Ciudad S; Puig E; Botzanowski T; Meigooni M; Arango AS; Do J; Mayzel M; Bayoumi M; Chaignepain S; Maglia G; Others. Aβ (1–42) Tetramer and Octamer Structures Reveal Edge Conductivity Pores as a Mechanism for Membrane Damage. Nat. Commun 2020, 11 (1), 1–14. [PubMed: 31911652]

(42). Yu L; Edalji R; Harlan JE; Holzman TF; Lopez AP; Labkovsky B; Hillen H; Barghorn S; Ebert U; Richardson PL; Miesbauer L; Solomon L; Bartley D; Walter K; Johnson RW; Hajduk PJ; Olejniczak ET Structural Characterization of a Soluble Amyloid Beta-Peptide Oligomer. Biochemistry 2009, 48 (9), 1870–1877. [PubMed: 19216516]

(43). Lendel C; Bjerring M; Dubnovitsky A; Kelly RT; Filippov A; Antzutkin ON; Nielsen NC; Härd T A Hexameric Peptide Barrel as Building Block of Amyloid-β Protofibrils. Angew. Chem. Int. Ed Engl 2014, 53 (47), 12756–12760. [PubMed: 25256598]

(44). Hamilton JA; Hillard CJ; Spector AA; Watkins PA Brain Uptake and Utilization of Fatty Acids, Lipids and Lipoproteins: Application to Neurological Disorders. J. Mol. Neurosci 2007, 33 (1), 2–11. [PubMed: 17901539]

(45). Bruce KD; Zsombok A; Eckel RH Lipid Processing in the Brain: A Key Regulator of Systemic Metabolism. Front. Endocrinol 2017, 8, 60.

(46). One reviewer has noted that interactions of Aβ with membrane components other than phospholipids, such as gangliosides and cholesterol, also play important roles in Aβ-membrane interactions.

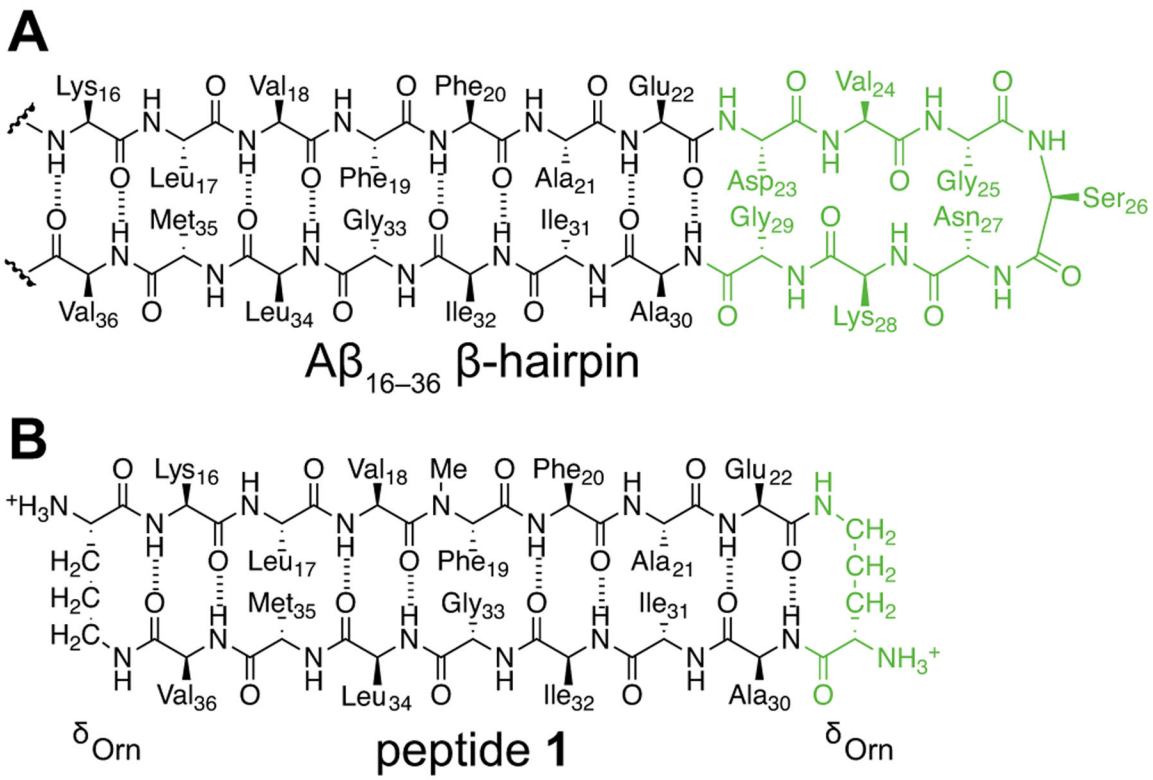

Figure 1.

Design of macrocyclic β-hairpin peptide **1** based on an $A\beta_{16–36}$ β-hairpin. (A) Chemical structure of an $A\beta_{16–36}$ β-hairpin. (B) Chemical structure of peptide **1**. The $^{\delta}$Orn that is colored green replaces the $A\beta_{23–29}$ loop.

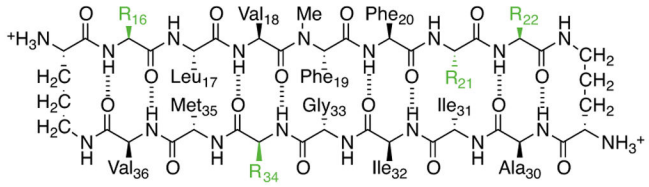

peptide	R_{16}	R_{21}	R_{22}	R_{34}	net charge at neutral pH
1	Lys	Ala	Glu	Leu	+2
$\mathbf{1_{E22D}}$	Lys	Ala	Asp	Leu	+2
$\mathbf{1_{E22G}}$	Lys	Ala	Gly	Leu	+3
$\mathbf{1_{E22Q}}$	Lys	Ala	Gln	Leu	+3
$\mathbf{1_{E22K}}$	Lys	Ala	Lys	Leu	+4
$\mathbf{1_{K16N}}$	Asn	Ala	Glu	Leu	+1
$\mathbf{1_{A21G}}$	Lys	Gly	Glu	Leu	+2
$\mathbf{1_{L34V}}$	Lys	Ala	Glu	Val	+2

Figure 2.

β-Hairpin peptides incorporating FAD mutations. Mutated residues are shown in green, R = residue. The net charge at neutral pH corresponds to the number of ammonium groups minus number of carboxylate groups.

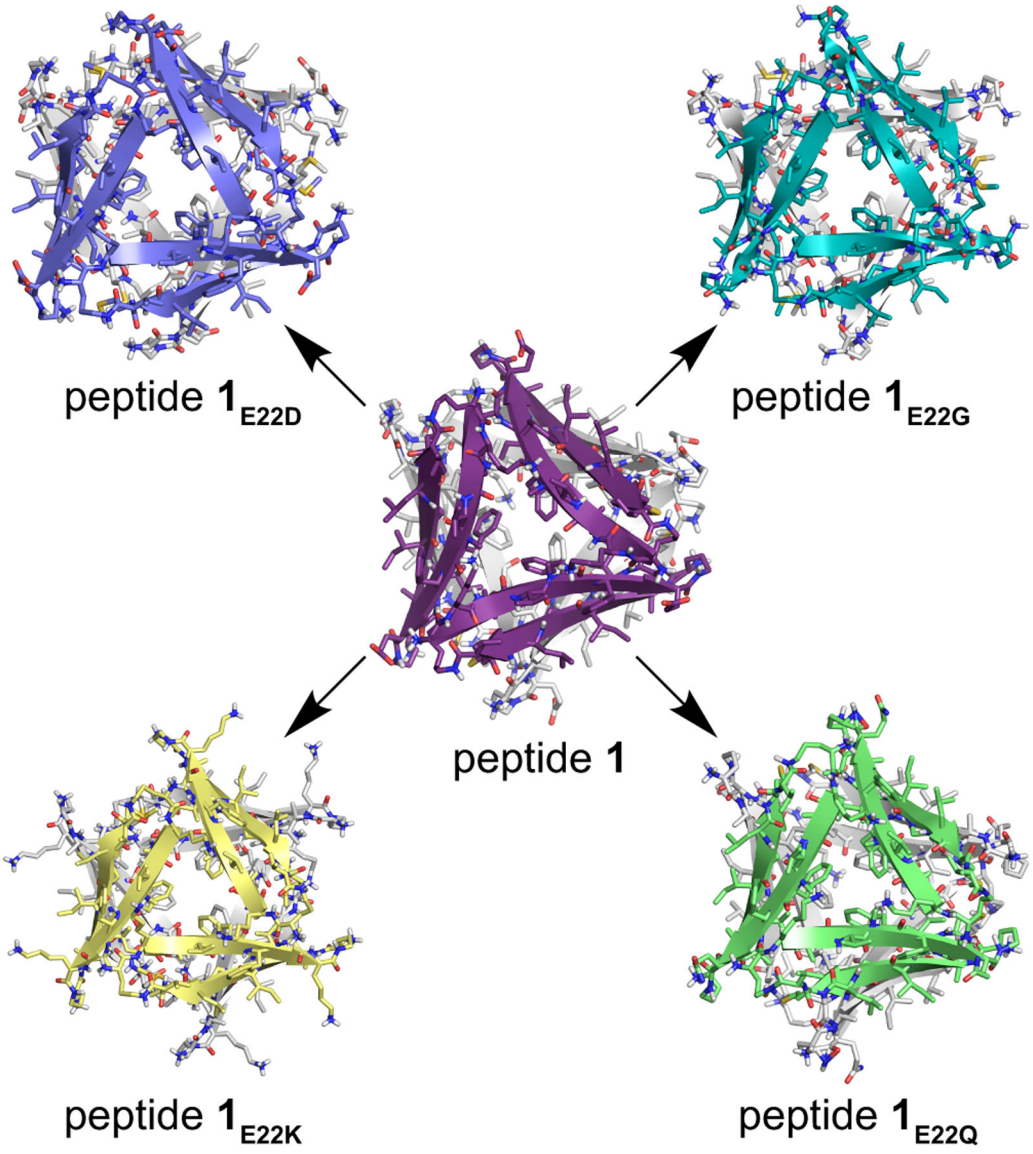

Figure 3.

X-ray crystallographic structures of the compact hexamers formed by peptides **1**, $\mathbf{1_{E22D}}$, $\mathbf{1_{E22G}}$, $\mathbf{1_{E22Q}}$, and $\mathbf{1_{E22K}}$. Peptide **1**, purple (PDB ID 5W4H); peptide $\mathbf{1_{E22D}}$, violet (PDB ID 7JQS); peptide $\mathbf{1_{E22G}}$, teal (PDB ID 7JQR); peptide $\mathbf{1_{E22Q}}$, light green (PDB ID 7JQU); peptide $\mathbf{1_{E22K}}$, yellow (PDB ID 7JQT).

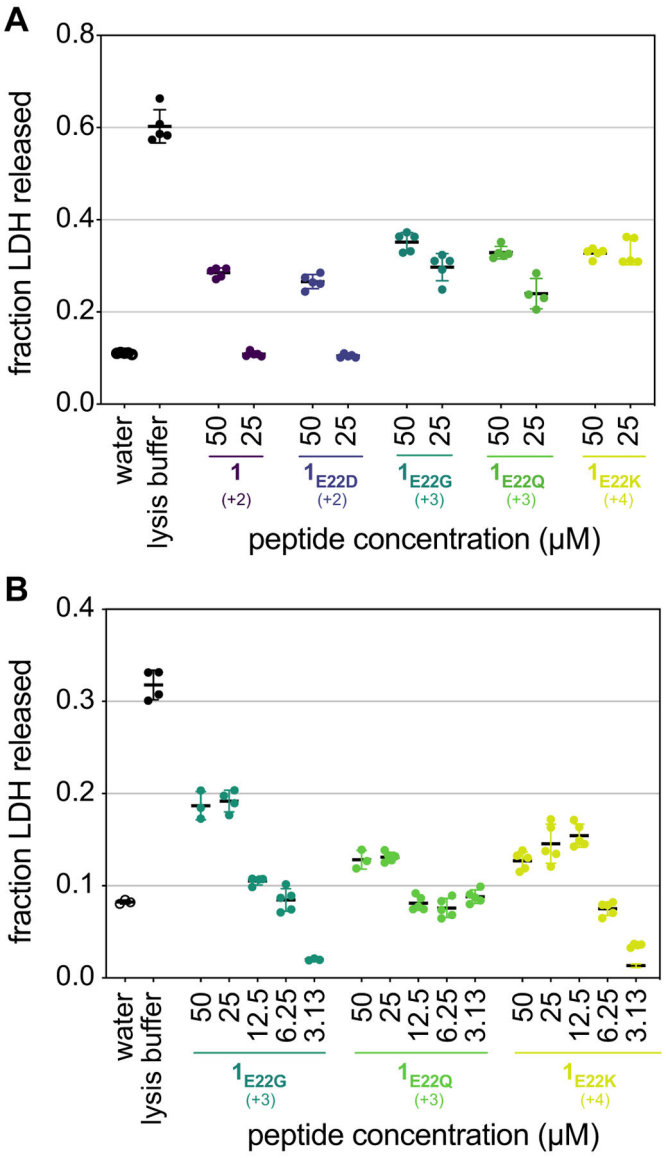

Figure 4.

Cytotoxicity of mutant peptides as assessed by LDH release assays. (A) Toxicity profiles of peptides **1**, $\mathbf{1_{E22D}}$, $\mathbf{1_{E22G}}$, $\mathbf{1_{E22Q}}$, and $\mathbf{1_{E22K}}$ at 50 and 25 μM. (B) Toxicity profiles of peptides $\mathbf{1_{E22G}}$, $\mathbf{1_{E22Q}}$, and $\mathbf{1_{E22K}}$ at 50, 25, 12.5, 6.25, and 3.13 μM. Each dot represents a single data point of five technical replicates, the horizontal black bars represent means, and the colored error bars represent standard deviations. Water served as a negative vehicle control and lysis buffer was the positive control.

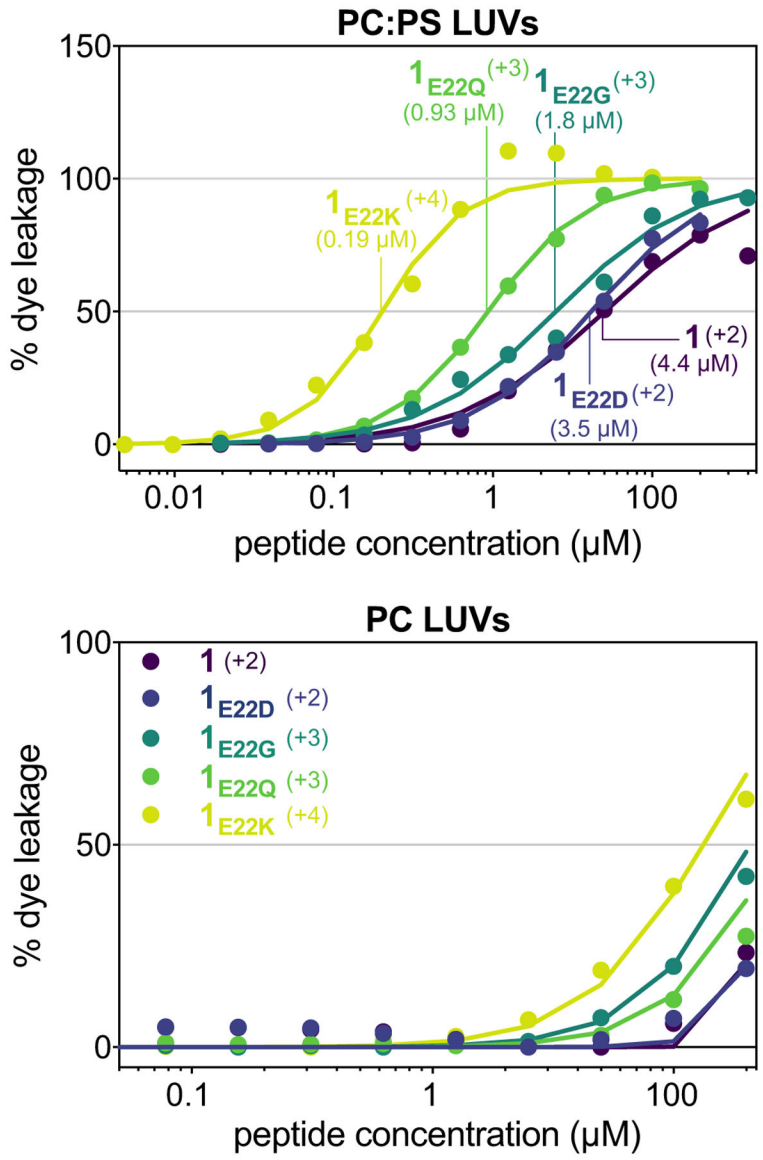

Figure 5.

Membrane destabilization by mutant peptides as determined by dye-leakage assays. Large unilamellar vesicles (LUVs) consisting of either 1:1 PC:PS (negatively charged) or PC (neutrally charged) lipids and containing calcein were treated with peptides **1**, $\mathbf{1}_{\mathbf{E22D}}$, $\mathbf{1}_{\mathbf{E22G}}$, $\mathbf{1}_{\mathbf{E22Q}}$, and $\mathbf{1}_{\mathbf{E22K}}$ at varying concentrations, and dye leakage was assessed by an increase in fluorescence. Peptides were prepared at various concentrations in Tris buffer (10 mM Tris pH 7.4, 150 mM NaCl, 1 mM EDTA) and incubated with LUVs containing 70 mM calcein. Fluorescence intensity was then measured at an emission wavelength of 520 nm and an excitation wavelength of 490 nm. The data were normalized by assigning the lysis buffer positive control as 100% dye leakage and the water negative control as 0% dye leakage. Data points represent averages of three replicate runs, error bars represent corresponding standard deviations (but are obscured by data points), and curves show nonlinear regression fits to the data. EC_{50} values for each peptide are shown under the peptide's name.

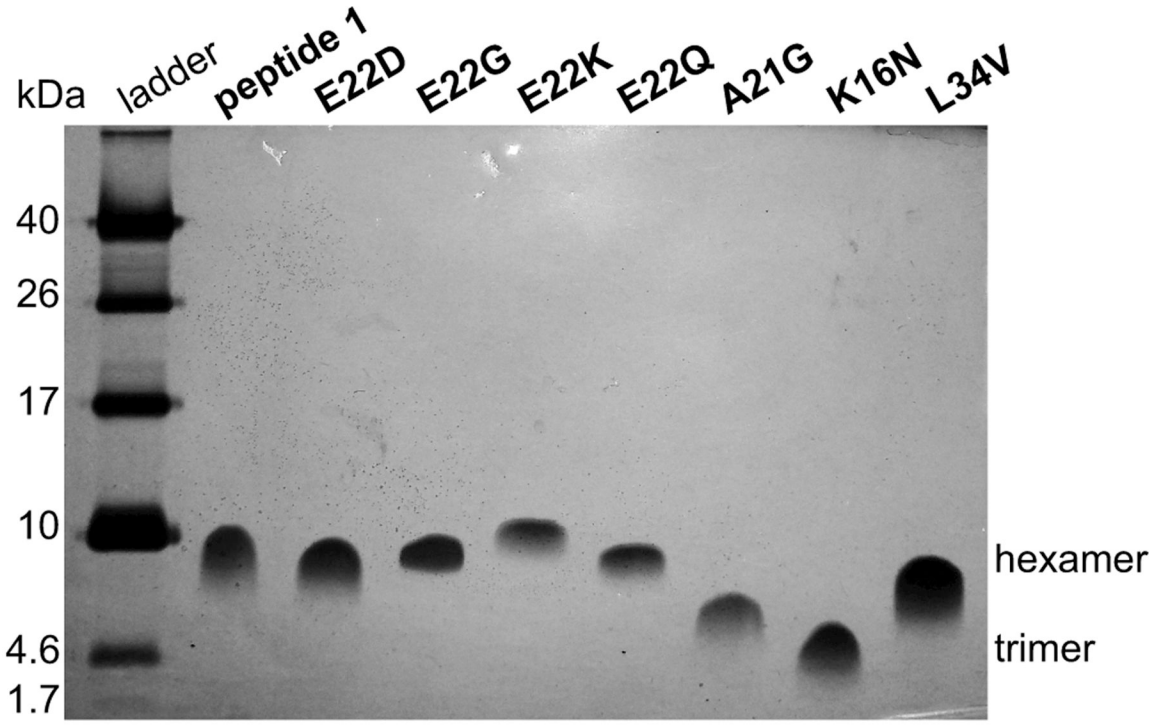

Figure 6.

Oligomeric assembly of peptide **1** and mutant peptides as visualized by SDS-PAGE. Mutant peptides were prepared to final concentrations of 0.2 mg/mL and 5 μL of each peptide was run on the gel. Peptide bands were visualized using silver staining.[23]

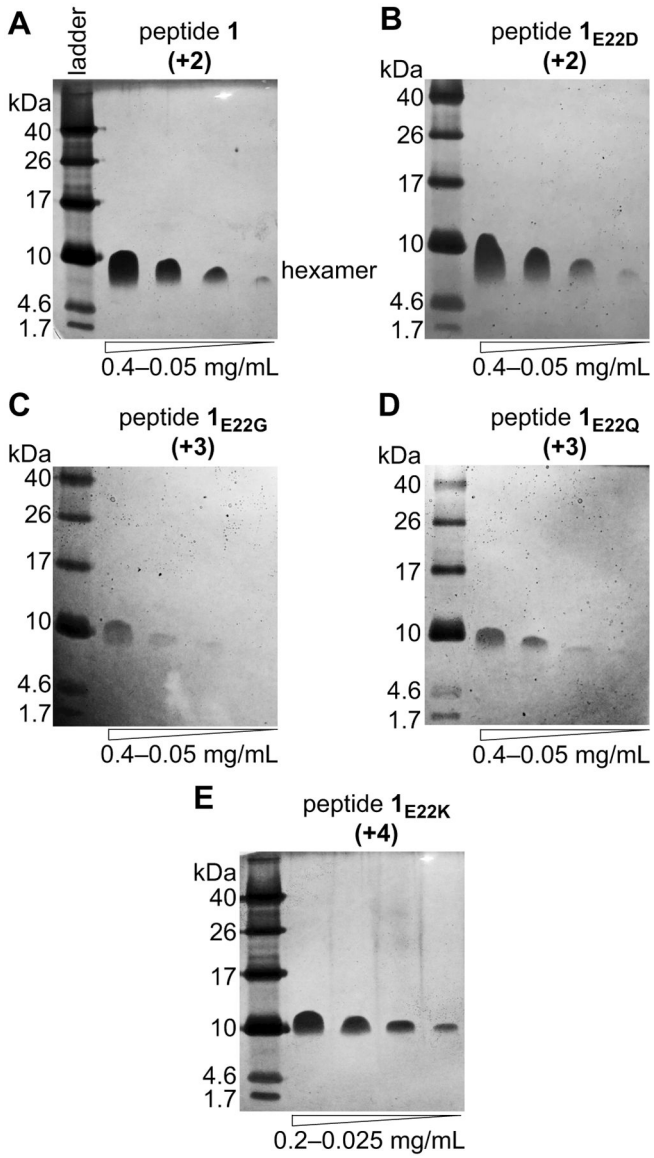

Figure 7.

Effect of concentration on E22 mutant peptide oligomer assembly as assessed by SDS-PAGE. A 5 μL aliquot of each peptide concentration was run on the gel. Peptide bands were visualized using silver staining: (A) Peptide **1**. (B) Peptide $\mathbf{1_{E22D}}$. (C) Peptide $\mathbf{1_{E22G}}$. (D) Peptide $\mathbf{1_{E22Q}}$. (E) Peptide $\mathbf{1_{E22K}}$.

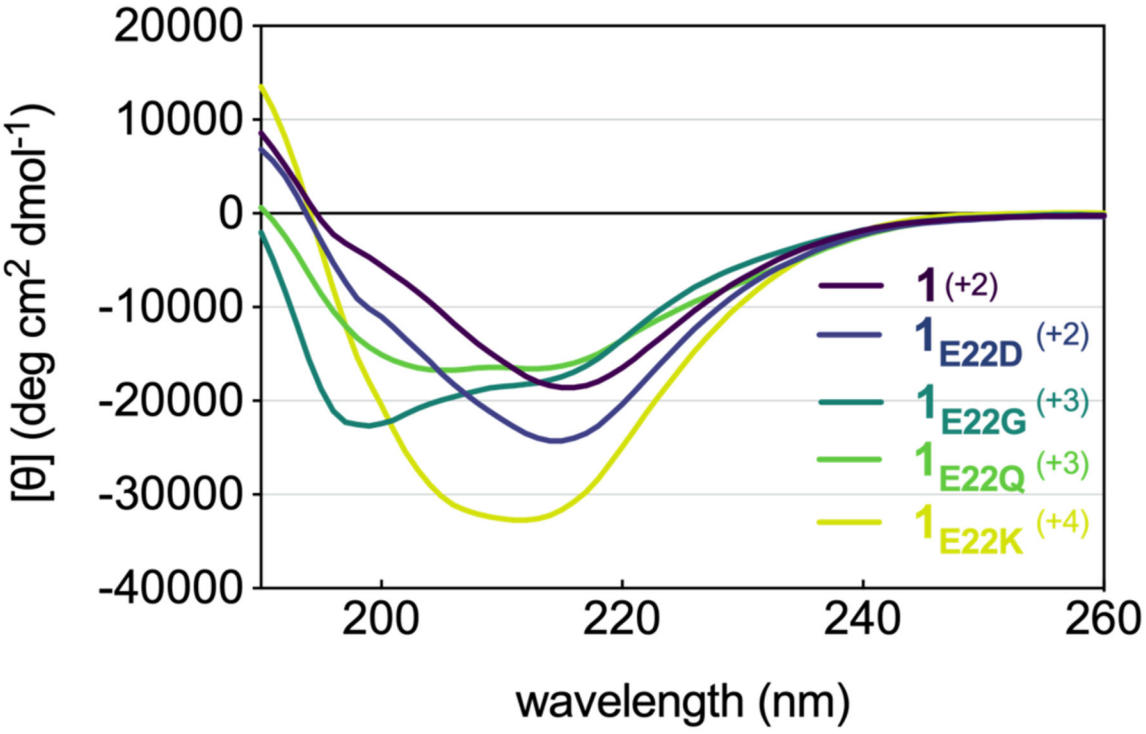

Figure 8.

CD spectra of peptides **1**, $\mathbf{1}_{\mathbf{E22D}}$, $\mathbf{1}_{\mathbf{E22G}}$, $\mathbf{1}_{\mathbf{E22Q}}$, and $\mathbf{1}_{\mathbf{E22K}}$. Spectra were acquired at peptide concentrations of 50 μM in 10 mM sodium phosphate buffer at pH 7.4 at 25°C.

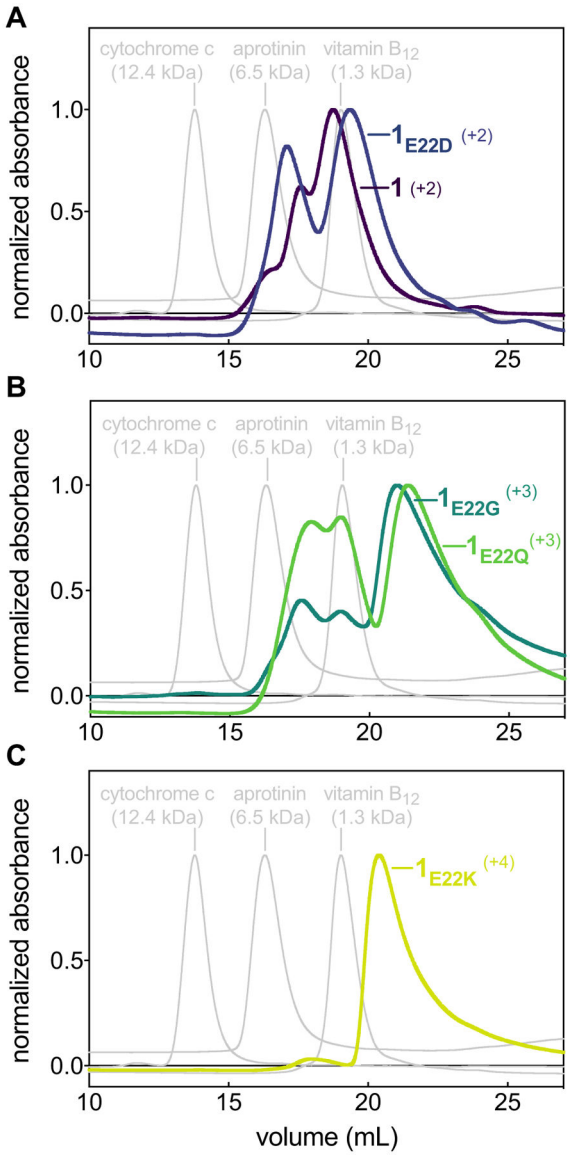

Figure 9.

SEC chromatograms of peptide **1** and $\mathbf{1_{E22D}}$ (A), peptides $\mathbf{1_{E22G}}$ and $\mathbf{1_{E22Q}}$ (B), and peptide $\mathbf{1_{E22K}}$ (C). Peptides were prepared at 1.0 mg/mL in 50 mM Tris buffer (pH 7.4) with 150 mM NaCl and run on a Superdex 75 10/300 column. Absorbance was recorded at 214 nm, and the chromatogram for each peptide was normalized. Cytochrome c, aprotinin, and vitamin B_{12} were included as molecular weight markers. Each mutant peptide has a molecular weight of ca. 1.8 kDa.

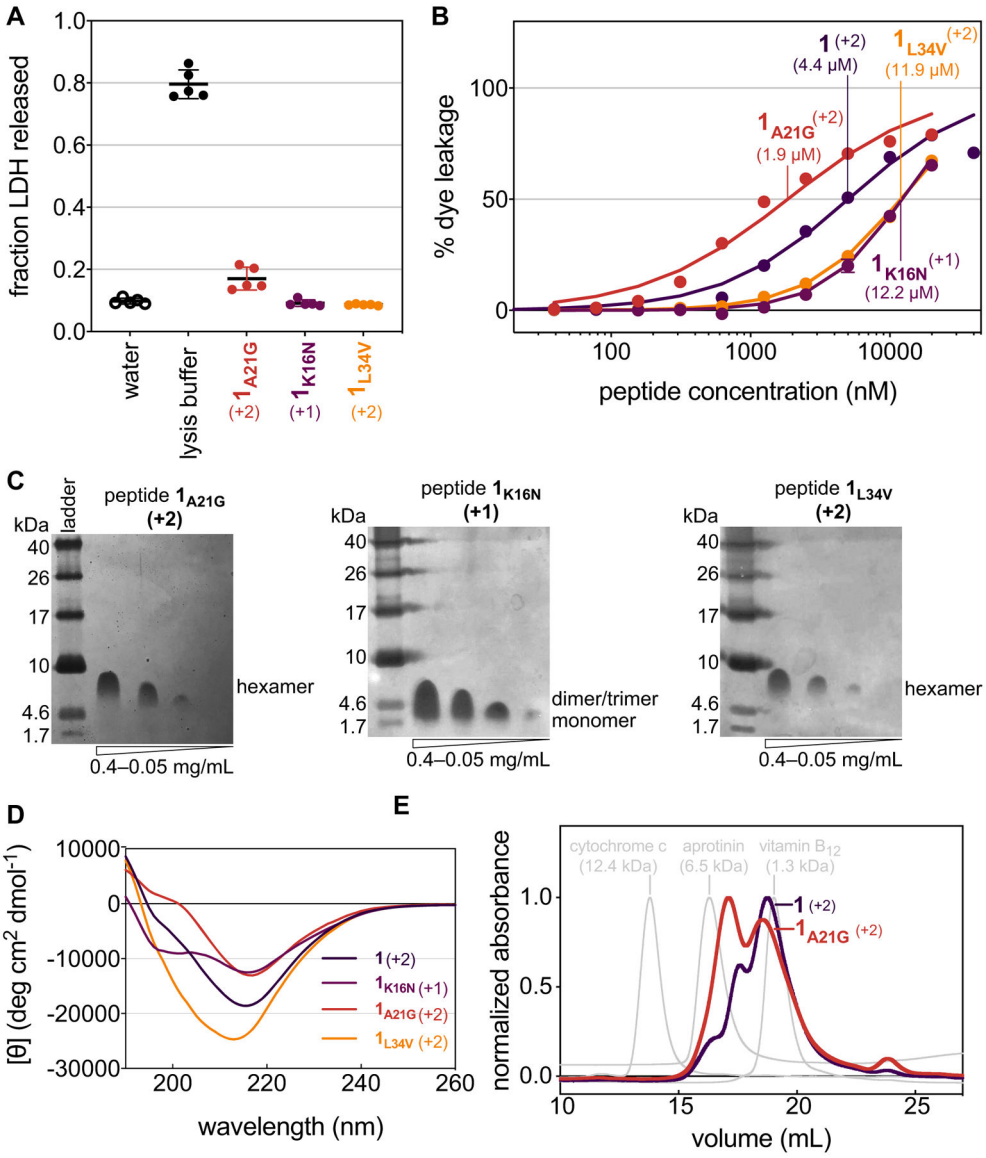

Figure 10.

Studies of peptides $\mathbf{1_{K16N}}$, $\mathbf{1_{A21G}}$, and $\mathbf{1_{L34V}}$. (A) Toxicities of peptides at 50 μM as assessed by LDH-release assays. (B) Membrane destabilization of mutant peptides as determined by dye-leakage assays with 1:1 PC:PS LUVs. (C) Effect of concentration on peptide oligomer assembly as assessed by SDS-PAGE. (D) CD spectra of peptides **1**, $\mathbf{1_{K16N}}$, $\mathbf{1_{A21G}}$, and $\mathbf{1_{L34V}}$ at 50 μM in 10 mM sodium phosphate buffer at pH 7.4 at 25°C. (E) SEC chromatograms of peptides **1** and $\mathbf{1_{A21G}}$.